

Active and Passive IRS Jointly Aided Communication: Deployment Design and Achievable Rate

Min Fu, *Member, IEEE* and Rui Zhang, *Fellow, IEEE*

Abstract—In this letter, we study the wireless point-to-point communication from a transmitter (Tx) to a receiver (Rx), which is jointly aided by an active intelligent reflecting surface (AIRS) and a passive IRS (PIRS). We consider two practical transmission schemes by deploying the two IRSs in different orders, namely, Tx→PIRS→AIRS→Rx (TPAR) and Tx→AIRS→PIRS→Rx (TAPR). Assuming line-of-sight channels, we derive the achievable rates for the two schemes by optimizing the placement of the AIRS with the location of the PIRS fixed. Our analysis shows that when the number of PIRS elements and/or the AIRS amplification power is small, the AIRS should be deployed closer to the Rx in both schemes, and TAPR outperforms TPAR with their respective optimized AIRS/PIRS placement. Simulation results validate our analysis and show the considerable performance gain achieved by the jointly optimized AIRS/PIRS deployment over the baseline double-PIRS system under the same power and IRS element budgets.

Index Terms—Intelligent reflecting surfaces (IRS), active IRS, double IRSs, IRS deployment, rate maximization.

I. INTRODUCTION

Intelligent reflecting surface (IRS) [1] has recently received significant attention from both academia and industry to improve the spectral and energy efficiency of future wireless networks cost-effectively. An IRS typically consists of an array of passive reflecting elements, each of which reflects the incident signal with a desired phase shift and/or amplitude. Unlike conventional active relays, passive IRSs (PIRSs) do not require costly transmit/receive radio-frequency (RF) chains and thus incur significantly lower power consumption [2]. As IRSs can be flexibly deployed in wireless networks to reconfigure wireless channels dynamically, they have been studied for achieving various functions such as coverage extension, rate enhancement, interference mitigation, etc (see, e.g., [1] and the references therein).

Most of the existing works (e.g., [3]–[6]) on IRS have considered the PIRS. Equipped with passive loads (positive resistance), PIRS reflects the incident signal with desired phase shift and reflection gain no larger than one. In addition, PIRSs operate in the full-duplex mode without amplification/processing noise or self-interference [1]. In particular, [3] showed that deploying a single PIRS with N reflecting

elements can lead to a squared power scaling order (i.e., $\mathcal{O}(N^2)$) of the reflected signal, which is even higher than that ($\mathcal{O}(N)$) of the active arrays. Furthermore, [4] proposed a double-PIRS system where N reflecting elements are equally allocated over two distributed PIRSs, which yields an even higher power scaling order ($\mathcal{O}(N^4)$) as compared to the single-PIRS system. Recently, wireless systems aided by multiple PIRSs with multiple signal reflections among them have also been investigated (see [7] and the references therein). Despite the low cost of PIRSs, their signal coverage performance is severely limited by the product-distance path-loss of the cascaded multi-reflection channel [7]. As a result, one PIRS needs to be allocated massive elements and/or deployed near the transmitter (Tx), the receiver (Rx), or other PIRSs in practice to make its signal reflection effective [7].

To address this issue with PIRS, the active IRS (AIRS) has emerged as a promising solution [8]–[12]. Equipped with negative resistance components connected to an additional power supply, AIRSs enable adjustable phase shifts like PIRSs as well as reflection amplitude with a gain larger than one. Compared to PIRSs, although AIRSs offer an amplification gain (that is typically lower than that of active relays with dedicated RF amplifiers), they also induce non-negligible amplification noise in their reflected signals [8]. In particular, given the IRS location and the total power budget, an AIRS was shown to achieve higher spectral efficiency [8], energy efficiency [11], and reliability [10] than its PIRS counterpart. Furthermore, with optimized AIRS/PIRS placements, [9] showed that an AIRS only provides a power scaling of $\mathcal{O}(N)$ with N active reflecting elements due to the amplification noise, but it achieves a higher rate than the PIRS when N is small or the AIRS amplification power is high. Nevertheless, the AIRS system design (e.g., AIRS deployment and amplification factor optimization) is more complicated since it needs to balance signal and noise amplification at the AIRS. The existing literature on AIRS has mainly compared its performance to PIRS. However, there has been limited work on exploring their joint use for further enhancing wireless communication performance.

In this letter, we study a new wireless communication system jointly aided by a pair of AIRS and PIRS, as illustrated in Fig. 1. To study IRS-enhanced link performance, we assume a pair of single-antenna Tx and Rx communicating through a double-reflection link via the two IRSs, while the other links between them are unavailable due to severe blockages. By deploying the two IRSs in different orders,

M. Fu is with the Department of Electrical and Computer Engineering, National University of Singapore, Singapore 117583 (e-mail: fumin@nus.edu.sg). R. Zhang is with the Chinese University of Hong Kong, Shenzhen, and Shenzhen Research Institute of Big Data, Shenzhen, China 518172 (e-mail: rzhang@cuhk.edu.cn). He is also with the Department of Electrical and Computer Engineering, National University of Singapore, Singapore 117583 (e-mail: elezhang@nus.edu.sg).

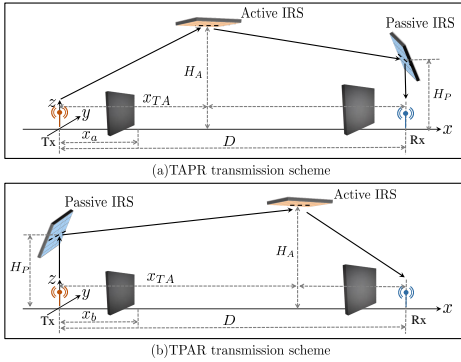


Fig. 1. The illustrations of AIRS and PIRS jointly aided wireless communication.

we consider two practical transmission schemes, which are Tx→PIRS→AIRS→Rx (TPAR) and Tx→AIRS→PIRS→Rx (TAPR) schemes, respectively (see Fig. 1). Furthermore, we assume that the two IRSs are properly deployed and thus they form a cascaded line-of-sight (LOS) link from the Tx to Rx via them successively. Under the above settings, we aim to characterize the achievable rates for the two schemes with their respective optimized AIRS/PIRS placement. Our analytic results show that for both schemes, when the number of PIRS elements is small, the AIRS should be placed closer to the Rx with decreasing amplification power. Besides, the TAPR scheme generally outperforms the TPAR scheme when the number of PIRS elements and/or the AIRS amplification power is small. Simulation results validate our analysis and demonstrate that the jointly optimized AIRS/PIRS deployment achieves a much higher rate than the baseline double-PIRS deployment under the same power and IRS element budgets.

II. SYSTEM MODEL AND PROBLEM FORMULATION

As illustrated in Fig. 1, a single-antenna Tx transmits data to a single-antenna Rx that is D meters (m) away. Under a three-dimensional Cartesian coordinate system, the locations of the Tx and Rx are denoted by $\mathbf{u}_T = (0, 0, 0)$ and $\mathbf{u}_R = (D, 0, 0)$, respectively. A pair of PIRS and AIRS are deployed between them to assist in their communication. The PIRS and AIRS are respectively placed at given altitudes, denoted by H_P and H_A , so that the Tx can communicate with the Rx via a double-reflection link through the two IRSs over three LOS channels. In particular, to reduce the product-distance path loss of the double-reflection channel, we assume that the PIRS is horizontally located above the Tx or Rx while the AIRS can be flexibly placed between them. We consider two transmission schemes by deploying the PIRS and AIRS in different orders, i.e., TAPR shown in Fig. 1(a) and TPAR shown in Fig. 1(b).

Let N_p and N_a denote the number of passive/active reflecting elements on the PIRS/AIRS, respectively. We further define \mathcal{N}_a and \mathcal{N}_p as the sets containing all the elements on the AIRS and PIRS, respectively. Let $\Theta_P = \text{diag}(\eta_{P,1}e^{j\phi_{P,1}}, \dots, \eta_{P,N_p}e^{j\phi_{P,N_p}})$ denote the reflection matrix of the PIRS, where $\eta_{P,n} \in [0, 1]$ and $\phi_{P,n} \in [0, 2\pi)$ denote respectively the reflection amplitude and phase-shift at passive element $n \in \mathcal{N}_p$. For maximal reflection of the PIRS and ease of practical implementation [1], we further set $\eta_{P,n} = 1, \forall n \in \mathcal{N}_p$. In addition, let $\Phi_A =$

$\text{diag}(\eta_{A,1}e^{j\phi_{A,1}}, \dots, \eta_{A,N_a}e^{j\phi_{A,N_a}})$ denote the reflection matrix of the AIRS, where $\eta_{A,n} \geq 1$ and $\phi_{A,n} \in [0, 2\pi)$ denote respectively the reflection amplitude and phase-shift at active element $n \in \mathcal{N}_a$. Since, under LOS channels, the transmitted signal arriving at each active element experiences the same pathloss, we assume that all active elements at the AIRS have the same amplification gain η [8], [9], i.e., $\eta_{A,n} = \eta, \forall n \in \mathcal{N}_a$. Moreover, different from the PIRS that reflects signals without incurring amplification noise, the AIRS generates non-negligible amplification noise at all reflecting elements, which is denoted by $\mathbf{n}_a \in \mathbb{C}^{N_a \times 1}$ and assumed to follow the independent circularly symmetric complex Gaussian distribution, i.e., $\mathbf{n}_a \sim \mathcal{CN}(\mathbf{0}_{N_a}, \sigma_P^2 \mathbf{I}_{N_a})$ with power σ_P^2 .

A. TAPR Transmission Scheme

First, we consider the TAPR scheme with the PIRS fixed above the Rx, as shown in Fig. 1(a).

1) *Signal model*: Denoting the Tx-AIRS horizontal distance as x_{TA} , the locations of the PIRS/AIRS are represented by $\mathbf{u}_P = (D, 0, H_P)$ and $\mathbf{u}_A = (x_{TA}, 0, H_A)$, respectively. Thus, the distances between the Rx and PIRS, the Tx and AIRS, and the AIRS and PIRS are respectively given by

$$d_{PR} = H_P, d_{TA}(x_{TA}) = \sqrt{x_{TA}^2 + H_A^2}, \quad (1)$$

$$d_{AP}(x_{TA}) = \sqrt{(D - x_{TA})^2 + (H_P - H_A)^2}, \quad (2)$$

where x_{TA} is considered as the design variable.

Let $\mathbf{g}_{TA} \in \mathbb{C}^{N_a \times 1}$, $\mathbf{S}_{AP} \in \mathbb{C}^{N_p \times N_a}$, and $\mathbf{h}_{RP}^H \in \mathbb{C}^{1 \times N_p}$ denote the baseband equivalent LOS channels for Tx→AIRS, AIRS→PIRS, and PIRS→Rx links, respectively. Before modeling LOS channels, we first define the one-dimensional steering vector function for a uniform linear array (ULA) as

$$\mathbf{e}(\theta, M') = [1, e^{-j\pi\theta}, \dots, e^{-j\pi(M'-1)\theta}]^T \in \mathbb{C}^{M' \times 1}, \quad (3)$$

where θ denotes the constant phase-shift difference between the signals at two adjacent elements and M' denotes the size of the ULA. For the uniform planar array (UPA) model, each array response vector can be expressed as the Kronecker product of two steering vector functions in the x-axis and y-axis directions, respectively. For example, the array response vector for the UPA from the Tx to AIRS is expressed as

$$\mathbf{a}_{TA}(\theta_{TA}, \vartheta_{TA}, N_a) = \mathbf{e}\left(\frac{2\Delta_A}{\lambda} \sin(\theta_{TA}) \cos(\vartheta_{TA}), N_{a,x}\right) \otimes \mathbf{e}\left(\frac{2\Delta_A}{\lambda} \sin(\theta_{TA}) \sin(\vartheta_{TA}), N_{a,y}\right) \in \mathbb{C}^{N_a \times 1}, \quad (4)$$

where λ denotes the signal wavelength, Δ_A denotes the element space at the AIRS, $(\theta_{TA}, \vartheta_{TA})$ is the angle-of-arrival pair, and $N_{a,x}$ and $N_{a,y}$ denote the number of horizontal/vertical elements at the AIRS with $N_a = N_{a,x} \times N_{a,y}$. As such, \mathbf{S}_{PA} , \mathbf{g}_{AT} , and \mathbf{h}_{RP}^H are respectively given by

$$\mathbf{S}_{AP} = \frac{\sqrt{\beta}}{d_{AP}} e^{-\frac{j2\pi d_{AP}}{\lambda}} \bar{\mathbf{s}}_{AP} \bar{\mathbf{s}}_{PA}^H, \quad (5)$$

$$\mathbf{g}_{TA} = \frac{\sqrt{\beta}}{d_{TA}} e^{-\frac{j2\pi d_{TA}}{\lambda}} \bar{\mathbf{g}}_{TA}, \mathbf{h}_{RP}^H = \frac{\sqrt{\beta}}{H_P} e^{-\frac{j2\pi H_P}{\lambda}} \bar{\mathbf{h}}_{RP}^H, \quad (6)$$

where β denotes the reference channel power at a distance of 1 m, $\bar{\mathbf{s}}_{AP} = \mathbf{a}_{AP}(\theta_{AP}, \vartheta_{AP}, N_p)$, $\bar{\mathbf{s}}_{PA} = \mathbf{a}_{PA}(\theta_{PA}, \vartheta_{PA}, N_a)$, $\bar{\mathbf{g}}_{TA} = \mathbf{a}_{TA}(\theta_{TA}, \vartheta_{TA}, N_a)$, and $\bar{\mathbf{h}}_{RP} = \mathbf{a}_{RP}(\theta_{RP}, \vartheta_{RP}, N_p)$.

Though the Tx→AIRS→PIRS→Rx reflecting link, the signal received at the Rx is given by

$$\begin{aligned} y_a &= \mathbf{h}_{\text{RP}}^H \Theta_P \mathbf{S}_{\text{AP}} \eta \Theta_A (\mathbf{g}_{\text{TA}} s + \mathbf{n}_a) + e \\ &= \underbrace{\mathbf{h}_{\text{RP}}^H \Theta_P \mathbf{S}_{\text{AP}} \eta \Theta_A \mathbf{g}_{\text{TA}} s}_{\text{Double-reflected signal}} + \underbrace{\mathbf{h}_{\text{RP}}^H \Theta_P \mathbf{S}_{\text{AP}} \eta \Theta_A \mathbf{n}_a}_{\text{Noise introduced by the AIRS}} + e, \end{aligned} \quad (7)$$

where s denotes the transmitted signal with power P_t of the Tx, and e denotes the additive white Gaussian noise at the Rx with power σ^2 . As observed from (7), the two IRSs can jointly enhance the double-reflected signal power whereas the AIRS introduces additional amplification noise. The received signal-to-noise ratio (SNR) at the Rx is expressed as

$$\text{SNR}_a(\Theta_A, \Theta_P, \eta, x_{TA}) = \frac{\|\mathbf{h}_{\text{RP}}^H \Theta_P \mathbf{S}_{\text{AP}} \eta \Theta_A \mathbf{g}_{\text{TA}}\|^2 P_t}{\|\mathbf{h}_{\text{RP}}^H \Theta_P \mathbf{S}_{\text{AP}} \eta \Theta_A\|^2 \sigma_F^2 + \sigma^2}, \quad (8)$$

and the achievable rate (in bits per second per Hertz or bps/Hz) for the TAPR scheme is given by

$$R_a = \log_2(1 + \text{SNR}_a(\Theta_A, \Theta_P, \eta, x_{TA})). \quad (9)$$

To avoid the impractical case where the AIRS attenuates the signal, the amplification factor needs to satisfy

$$\eta \geq 1. \quad (10)$$

Denoting P_F as the given amplification power budget of the AIRS, the amplification power constraint over the signal reflected by the AIRS is given by [8], [9]

$$\eta^2 (P_t \|\Theta_A \mathbf{g}_{\text{TA}}\|^2 + \sigma_F^2 \|\Theta_A \mathbf{I}_{N_a}\|^2) \leq P_F. \quad (11)$$

2) *Problem formulation:* We aim to maximize the achievable rate for the Rx by jointly optimizing the reflection matrices at the PIRS/AIRS (i.e., Θ_P and $\eta \Theta_A$) and the AIRS deployment (i.e., x_{TA}). Accordingly, for the TAPR scheme, the optimization problem is formulated as

$$\underset{\Theta_A, \Theta_P, \eta, x_{TA}}{\text{maximize}} \quad \log_2(1 + \text{SNR}_a(\Theta_A, \Theta_P, \eta, x_{TA}))$$

$$\text{subject to} \quad |\Theta_P(n, n)| = 1, \forall n \in \mathcal{N}_p, \quad (12a)$$

$$|\Theta_A(n, n)| = 1, \forall n \in \mathcal{N}_a, \quad (12b)$$

$$0 \leq x_{TA} \leq D, \quad (12c)$$

Constraints (10), (11).

Since the objective function is increasing with η , the amplification power constraint in (11) needs to be active at the optimal solution of problem (12). Furthermore, the amplification power in (11) is independent of the phase values in Θ_A and Θ_P while the objective function of problem (12) is maximized by designing the phases of the AIRS and PIRS to align in the cascaded Tx-AIRS-PIRS-Rx channel. Therefore, for given x_{TA} , the optimal phase design of the AIRS/PIRS and the optimal amplification factor are respectively given by

$$\Theta_A(n, n) = e^{-j(\angle[\bar{\mathbf{s}}_{PA}]_n + \angle[\mathbf{g}_{\text{TA}}]_n)}, \quad (13)$$

$$\Theta_P(n, n) = e^{-j(\angle[\bar{\mathbf{s}}_{AP}]_n + \angle[\mathbf{h}_{\text{PR}}^H]_n)}, \quad (14)$$

$$\eta = \sqrt{P_F d_{TA}^2(x_{TA}) / (P_t N_a \beta + d_{TA}^2(x_{TA}) \sigma_F^2 N_a)}. \quad (15)$$

With η , Θ_A , and Θ_P given in the above, the receiver SNR in (8) is rewritten as

$$\begin{aligned} &\text{SNR}_a(x_{TA}) \\ &= \frac{P_t P_F \beta^2 N_a N_p^2}{C_1 d_{TA}^2(x_{TA}) + C_2 d_{AP}^2(x_{TA}) + C_3 d_{TA}^2(x_{TA}) d_{AP}^2(x_{TA})}, \end{aligned} \quad (16)$$

where $C_1 = \sigma_F^2 P_F \beta N_p^2$, $C_2 = \sigma^2 P_t H_P^2$, and $C_3 = H_P^2 \sigma_F^2 \sigma^2 / \beta$. After substituting (13), (14), and (15) into (12), problem (12) is equivalent to the following,

$$\begin{aligned} &\underset{x_{TA}}{\text{maximize}} \quad \log_2(1 + \text{SNR}_a(x_{TA})) \\ &\text{subject to} \quad x_a \leq x_{TA} \leq D, \end{aligned} \quad (17a)$$

where constraint (17a) corresponds to (10) in problem (12) and

$$x_a = \sqrt{\max\{0, N_a \beta P_t / (P_F - N_a \sigma_F^2) - H_A^2\}}. \quad (18)$$

Although the optimal solution to problem (17) is difficult to be characterized in closed form due to the complicated expression of $\text{SNR}_a(x_{TA})$, its value can be obtained by using a one-dimensional search over $x_{TA} \in [x_a, D]$. In the following, we first characterize the effects of AIRS amplification power and the number of PIRS elements on the optimal AIRS placement.

Lemma 1. The optimal Tx-AIRS horizontal distance (i.e., x_{TA}^*) to problem (17) is *non-increasing* with P_F and monotonically *decreasing* with N_p .

Proof. First, it can be shown that x_a is non-increasing with P_F . In addition, it is observed from the first denominator term of $\text{SNR}_a(x_{TA})$ that C_1 and $d_{TA}(x_{TA})$ monotonically increases with both P_F and x_{TA} . If constraint (17a) is not considered, x_{TA} should be decreased to maximize the objective function of problem (17) as P_F increases. Thus, the optimal solution x_{TA}^* is non-increasing with P_F .

Second, it can be shown that x_a is independent of N_p while C_1 monotonically increases with N_p . If without constraint (17a), x_{TA} should be decreased to maximize the objective function of problem (17) as N_p increases. Thus, the optimal solution x_{TA}^* is decreasing with N_p .

This thus completes the proof. \square

Lemma 1 is expected for the TAPR scheme in order to balance the received signal power maximization and the AIRS-induced noise minimization. On one hand, as observed from (15), the AIRS should be deployed farther away from the Tx as P_F decreases, so that the AIRS can provide a higher amplification factor with $\eta > 1$ while the path loss of the cascaded channel can be reduced to maximize the received signal power. On the other hand, based on (8), although the received signal power increases with the number of PIRS reflecting elements (i.e., N_p), the AIRS-induced noise is also increased. As such, as N_p increases, the AIRS has to be deployed closer to the Tx to attenuate the AIRS-PIRS channel for suppressing its induced noise power at the Rx.

B. TPAR Transmission Scheme

Next, we consider the TPAR transmission scheme with the PIRS fixed above the Tx, as shown in Fig. 1(b).

Similarly to the TAPR case, denoting the horizontal distance between the Tx and AIRS as x_{TA} , the locations of the PIRS/AIRS are represented by $\mathbf{u}_P = (0, 0, H_P)$ and $\mathbf{u}_A = (x_{TA}, 0, H_A)$, respectively. The signal model of TPAR is also similar to that of TAPR, while the expressions of the AIRS amplification noise and its power constraint are different since the order of the AIRS/PIRS placements is reversed. The detailed expressions are omitted for brevity.

Similarly to the design of η , Θ_A , and Θ_P in the TAPR scheme, the expressions of the AIRS amplification factor and receiver SNR in the case of TPAR are respectively given by

$$\eta = \sqrt{P_F d_{AP}^2 / (P_t N_a \beta^2 N_p^2 / H_P^2 + d_{AP}^2 \sigma_F^2 N_a)}, \quad (19)$$

$\text{SNR}_b(x_{TA})$

$$= \frac{N_a \beta^2 N_p^2 P_t P_F}{C_2 / a d_{AP}^2(x_{TA}) + a C_1 d_{AR}^2(x_{TA}) + C_3 d_{AP}^2(x_{TA}) d_{AR}^2(x_{TA})}, \quad (20)$$

where $a = \frac{P_t \sigma^2}{P_F \sigma_F^2}$. As a result, the optimization problem of the TPAR scheme is formulated as

$$\begin{aligned} & \underset{x_{TA}}{\text{maximize}} \quad \log_2(1 + \text{SNR}_b(x_{TA})) \\ & \text{subject to} \quad x_b \leq x_{TA} \leq D, \end{aligned} \quad (21a)$$

where constraint (21a) is due to the amplification power constraint at the AIRS, and

$$x_b = \sqrt{\max\{0, N_a N_p^2 \beta^2 P_t / ((P_F - N_a \sigma_F^2) H_P^2) - (H_P - H_A)^2\}}.$$

Similarly to problem (17), the optimal solution of problem (21) can also be obtained by using the one-dimensional search over $x_{TA} \in [x_b, D]$. Likewise, we have the following lemma for the TPAR scheme.

Lemma 2. The optimal Tx-AIRS horizontal distance (i.e., x_{TA}^*) to problem (21) is *non-increasing* with P_F and monotonically *increasing* with N_p .

Proof. The proof is similar to that of Lemma 1, and thus omitted for brevity. \square

Lemma 2 can be intuitively understood for the TPAR scheme. The AIRS-induced noise is independent of the number of PIRS reflecting elements. As observed from (19), with a smaller P_F and/or a larger N_p , the AIRS should be deployed closer to the Rx to provide a higher amplification factor with $\eta > 1$ and reduce the path loss of the cascaded channel, thus increasing the signal power at the Rx.

III. LOW-COMPLEXITY PLACEMENT DESIGN AND PERFORMANCE COMPARISON

In this section, we present suboptimal AIRS deployment solutions in closed-form for the TAPR and TPAR schemes, respectively. Based on these results, we compare the performance of the two schemes in terms of achievable rate.

A. Suboptimal Solutions

First, to simplify problems (17) and (21), we present a useful lemma as follows (for which the proof is omitted for brevity).

Lemma 3. Given $D \gg \max\{H_A, H_P\}$, we have $C_1 d_{TA}^2(x_{TA}) + C_2 d_{AP}^2(x_{TA}) \gg C_3 d_{TA}^2(x_{TA}) d_{AP}^2(x_{TA})$ and $C_2 / a d_{AP}^2(x_{TA}) + a C_1 d_{AR}^2(x_{TA}) \gg C_3 d_{AP}^2(x_{TA}) d_{AR}^2(x_{TA})$, $\forall x_{TA} \in [0, D]$, if

$$\min\left\{\frac{\sqrt{\beta} N_p \sqrt{P_t \beta}}{H_p \sigma_F} + \frac{\sqrt{P_F \beta}}{\sigma}, \frac{\sqrt{\beta} N_p \sqrt{P_F \beta}}{H_p \sigma} + \frac{\sqrt{P_t \beta}}{\sigma_F}\right\} \gg D. \quad (22)$$

1) *TAPR Scheme:* When condition (22) is satisfied, R_a in problem (17) can be approximated as $\bar{R}_a = \log_2(1 + \text{SNR}_a)$,

where $\overline{\text{SNR}}_a = \frac{P_t P_F \beta^2 N_a N_p^2}{C_1 x_{TA}^2 + C_2 (D - x_{TA})^2}$. Therefore, problem (17) is approximated as

$$\begin{aligned} & \underset{x_{TA}}{\text{maximize}} \quad \log_2\left(1 + \frac{P_t P_F \beta^2 N_a N_p^2}{C_1 x_{TA}^2 + C_2 (D - x_{TA})^2}\right) \\ & \text{subject to} \quad \text{constraint (17a)}. \end{aligned} \quad (23)$$

By setting the first derivative of the objective function of (23) with respect to x_{TA} to zero and then projecting it into the feasible set of problem (23), the optimal solution to problem (23) can be obtained as

$$x_{TA}^a = \max\left\{\frac{aD}{a+b}, x_a\right\}, \quad (24)$$

where $a = \frac{P_t \sigma^2}{P_F \sigma_F^2}$ and $b = \frac{\beta N_p^2}{H_P^2}$. Note that when $\frac{aD}{a+b} > x_a$, the amplification factor (i.e., η) in problem (12) is larger than 1. Given $\eta > 1$, the receiver SNR is approximated as

$$\overline{\text{SNR}}_a = \frac{P_F \beta N_a}{D^2 \sigma^2} (a+b) = \frac{\beta N_a}{D^2} \left(\frac{P_t}{\sigma_F^2} + \frac{P_F N_p^2 \beta}{\sigma^2 H_P}\right). \quad (25)$$

2) *TPAR Scheme:* Similarly, based on Lemma 3, problem (21) is approximated as

$$\begin{aligned} & \underset{x_{TA}}{\text{maximize}} \quad \log_2\left(1 + \frac{P_t P_F \beta^2 N_a N_p^2}{1/a C_2 x_{TA}^2 + a C_1 (D - x_{TA})^2}\right) \\ & \text{subject to} \quad \text{constraint (21a)}. \end{aligned} \quad (26)$$

Similarly to problem (23), the optimal solution to problem (26) is obtained as

$$x_{TA}^b = \max\left\{\frac{abD}{ab+1}, x_b\right\}. \quad (27)$$

Given $\eta > 1$, the approximated receiver SNR is given by

$$\overline{\text{SNR}}_b = \frac{P_F \beta N_a}{D^2 \sigma^2} (ab+1) = \frac{\beta N_a}{D^2} \left(\frac{P_t N_p^2 \beta}{\sigma_F^2 H_P} + \frac{P_F}{\sigma^2}\right). \quad (28)$$

B. Comparisons between TPAR and TAPR

With the suboptimal AIRS deployments given in (24) and (27), the achievable rates for the TPAR and TAPR schemes are compared as follows.

Proposition 1. Given $\eta > 1$ and $N_p \leq \frac{H_P}{\sqrt{\beta}}$, the achievable rate of the TPAR scheme is no less than that of the TAPR scheme, i.e., $\bar{R}_a \geq \bar{R}_b$, if

$$P_F \leq \frac{P_t \sigma^2}{\sigma_F^2}. \quad (29)$$

Otherwise, $\bar{R}_a < \bar{R}_b$. The result is reversed when $N_p \geq \frac{H_P}{\sqrt{\beta}}$.

Proof. Comparing \bar{R}_a and \bar{R}_b is equivalent to comparing $\overline{\text{SNR}}_a$ and $\overline{\text{SNR}}_b$. Thus, with $\eta > 1$, based on (25) and (28), we have

$$\begin{aligned} \overline{\text{SNR}}_a - \overline{\text{SNR}}_b &= \frac{P_F \beta N_a}{D^2 \sigma^2} (a+b-ab-1) \\ &= \frac{\beta N_a}{D^2} \frac{\left(\frac{P_t}{\sigma_F^2} - \frac{P_F}{\sigma^2}\right) (H_P^2 - N_p^2 \beta)}{H_P^2}. \end{aligned} \quad (30)$$

Based on (30), we can conclude that $\bar{R}_a \geq \bar{R}_b$, if

$$N_p \leq \frac{H_P}{\sqrt{\beta}}, \frac{P_F}{\sigma^2} \leq \frac{P_t}{\sigma_F^2}, \text{ or } N_p \geq \frac{H_P}{\sqrt{\beta}}, \frac{P_F}{\sigma^2} \geq \frac{P_t}{\sigma_F^2}. \quad (31)$$

Otherwise, $\bar{R}_a < \bar{R}_b$. This thus completes the proof. \square

IV. NUMERICAL RESULTS

In this section, we present numerical results to compare the rate performance of the TAPR and TPAR schemes in an AIRS-PIRS jointly aided communication system. If not specified

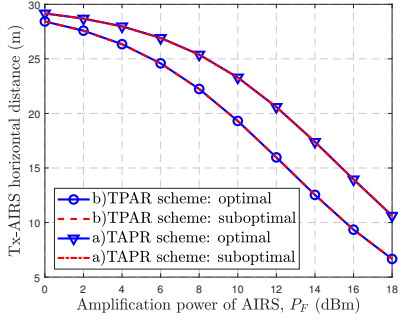


Fig. 2. Optimal AIRS placement versus amplification power of the AIRS.

otherwise, the simulation parameters are set as follows. The AIRS and PIRS are assumed to be deployed at altitudes of $H_A = 6$ m and $H_P = 5$ m, respectively. The carrier frequency is 3.5 GHz and thus the reference channel gain is $\beta = (\lambda/4\pi)^2 = -43$ dB, with the carrier wavelength $\lambda = 0.087$ m. Other parameters are set as $D = 30$ m, $P_t = 20$ dBm, $\sigma^2 = -80$ dBm, and $\sigma_F^2 = 4\sigma^2 = -74$ dBm. Under our simulation setup, we consider a limited budget of reflecting elements with $N_a < N_p < \frac{H_P}{\sqrt{\beta}} \approx 700$ (see Proposition 1). The numbers of AIRS and PIRS elements are thus fixed as $N_a = 450$ and $N_p = 600$, respectively.

For performance comparison, we consider a benchmark case with double PIRSs [4]. Specifically, both PIRSs are equally equipped with $(N_a + N_p)/2$ elements and deployed above the Tx and Rx, respectively. Furthermore, the transmit power of Tx in the double-PIRS system is $(P_t + P_F)$. As such, it is fair to compare it with the AIRS-PIRS jointly aided system. For the latter, we also consider four fixed AIRS/PIRS deployments, where x_{AP} equals $D/2$ or D in both TAPR/TPAR schemes.

Fig. 2 shows the optimal Tx-AIRS horizontal distance versus AIRS amplification power. We observe that the optimal AIRS placement in both schemes is closer to the Rx (i.e., larger x_{TA}) as P_F decreases. This is consistent with Lemmas 1 and 2. Besides, the suboptimal deployment in both schemes is almost the same as the optimal one.

Fig. 3 compares the achievable rates versus AIRS amplification power. First, as P_F increases, we observe that the rate performance of all AIRS/PIRS deployment strategies in the AIRS-PIRS jointly aided system increases due to the more amplification gain from AIRS. However, the rate improvement for the Rx-side AIRS deployment in TPAR is marginal with P_F since the signal amplification at the AIRS is gradually counteracted by its induced amplification noise. Compared to these fixed deployment strategies, the AIRS deployment design in both TAPR/TPAR schemes dynamically balances the signal and noise amplification at the AIRS and thus achieves further performance improvement. Furthermore, with the optimal AIRS placement, TAPR performs better than TPAR when $P_F < \frac{P_t \sigma^2}{\sigma_F^2}$, because it suffers less path loss of the cascaded channel and thus results in higher received power. These results are consistent with Proposition 1. In addition, thanks to the optimal AIRS/PIRS placement and the resulting amplification gain at AIRS, the AIRS-PIRS jointly aided system achieves a much higher rate than the baseline double-PIRS system under a limited IRS element budget.

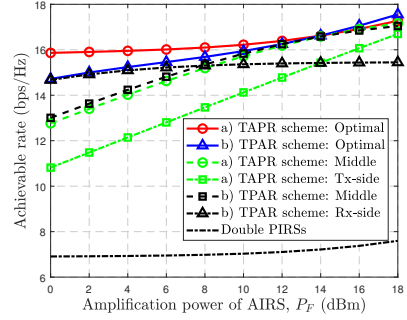


Fig. 3. Achievable rate versus amplification power of the AIRS.

V. CONCLUSION

In this letter, we studied a new AIRS-PIRS jointly aided wireless communication system. Under the LOS channel model, we analyzed the effects of the AIRS deployment in two transmission schemes (i.e., TAPR and TPAR) on their achievable rates. Our analysis revealed that the AIRS should be deployed closer to the Rx in both schemes, and TAPR achieves a higher rate than TPAR when the number of PIRS elements and/or AIRS amplification power is limited. Simulation results validated our analysis and demonstrated that our proposed system considerably outperforms the double-PIRS system in terms of achievable rate, and the performance gain highly depends on the AIRS/PIRS deployment.

REFERENCES

- [1] Q. Wu, S. Zhang, B. Zheng, C. You, and R. Zhang, "Intelligent reflecting surface-aided wireless communications: A tutorial," *IEEE Trans. Commun.*, vol. 69, no. 5, pp. 3313–3351, May 2021.
- [2] D. Renzo *et al.*, "Reconfigurable intelligent surfaces vs. relaying: Differences, similarities, and performance comparison," *IEEE Open J. Commun. Soc.*, vol. 1, pp. 798–807, Jun. 2020.
- [3] Q. Wu and R. Zhang, "Intelligent reflecting surface enhanced wireless network via joint active and passive beamforming," *IEEE Trans. Wireless Commun.*, vol. 18, no. 11, p. 5394–5409, Aug. 2019.
- [4] Y. Han, S. Zhang, L. Duan, and R. Zhang, "Double-IRS aided MIMO communication under LoS channels: Capacity maximization and scaling," *IEEE Trans. Commun.*, vol. 70, no. 4, pp. 2820–2837, Apr. 2022.
- [5] B. Zheng, C. You, and R. Zhang, "Double-IRS assisted multi-user MIMO: Cooperative passive beamforming design," *IEEE Trans. Wireless Commun.*, vol. 20, no. 7, pp. 4513–4526, Jul. 2021.
- [6] M. Fu, Y. Zhou, Y. Shi, and K. B. Letaief, "Reconfigurable intelligent surface empowered downlink non-orthogonal multiple access," *IEEE Trans. Commun.*, vol. 69, no. 6, pp. 3802–3817, Jun. 2021.
- [7] W. Mei, B. Zheng, C. You, and R. Zhang, "Intelligent reflecting surface-aided wireless networks: From single-reflection to multireflection design and optimization," *Proc. IEEE*, 2022, doi:10.1109/JPROC.2022.3170656.
- [8] R. Long, Y.-C. Liang, Y. Pei, and E. G. Larsson, "Active reconfigurable intelligent surface-aided wireless communications," *IEEE Trans. Wireless Commun.*, vol. 20, no. 8, pp. 4962–4975, Aug. 2021.
- [9] C. You and R. Zhang, "Wireless communication aided by intelligent reflecting surface: Active or passive?" *IEEE Wireless Commun. Lett.*, vol. 10, no. 12, pp. 2659–2663, Dec. 2021.
- [10] M. H. Khoshafa, T. M. N. Ngatched, M. H. Ahmed, and A. R. Ndjiongue, "Active reconfigurable intelligent surfaces-aided wireless communication system," *IEEE Commun. Lett.*, vol. 25, no. 11, pp. 3699–3703, Nov. 2021.
- [11] K. Liu, Z. Zhang, L. Dai, S. Xu, and F. Yang, "Active reconfigurable intelligent surface: Fully-connected or sub-connected?" *IEEE Commun. Lett.*, vol. 26, no. 1, pp. 167–171, Jan. 2022.
- [12] K. Zhi, C. Pan, H. Ren, K. K. Chai, and M. ElKashlan, "Active RIS versus passive RIS: Which is superior with the same power budget?" *IEEE Commun. Lett.*, vol. 26, no. 5, pp. 1150–1154, May 2022.